Supplementary Materials

Possible precipitates considered in thermodynamic modeling

In seawater-urine mixture, a number of phosphate and carbonate minerals might precipitate owing to the presence of magnesium, calcium, ammonium, phosphate, and carbonate species. Since Visual MINTEQ is only for calculation of chemical thermodynamics and does not incorporate kinetics, while P precipitation from urine typically finishes within a short residence time (in the order of hours, e.g., Musvoto et al. (2000); Tilley et al. (2008); Tang et al. (2015)), minerals with slow precipitation kinetics should be excluded from consideration. A brief literature review was thus conducted to determine the candidate precipitates.

Magnesium phosphates. In addition to struvite (magnesium ammonium phosphate), three other possible species of magnesium phosphates can precipitate in seawater-urine mixture: 1) newberyite (magnesium hydrogen phosphate trihydrate, $MgHPO_4 \cdot 3H_2O$); 2) $Mg_3(PO_4)_2 \cdot 22H_2O$; and 3) bobierrite ($Mg_3(PO_4)_2 \cdot 8H_2O$). Bobierrite and $Mg_3(PO_4)_2 \cdot 22H_2O$ precipitate significantly slower than struvite (Mamais et al., 1994). Newberyite precipitates at pH levels lower than 6.0 (Abbona et al., 1986), whereas the pH of urine ranges from 6.3 to 9.3, and that of seawater is generally around 8.0 (Table 1). As a result, struvite is expected to be the only possible crystalline form of magnesium phosphate in the seawater-urine mixture, and was included in the thermodynamics calculation.

Calcium phosphates. Six forms of crystallized calcium phosphate can precipitate from seawater-urine mixture containing calcium and phosphate: 1) amorphous calcium phosphate ($Ca_9(PO_4)_6 \cdot nH_2O$, ACP); 2) hydroxyapatite ($Ca_{10}(PO_4)_6(OH)_2$, HA); 3) tricalcium phosphate ($Ca_3(PO_4)_2$, TCP); 4) dicalcium phosphate anhydrate ($CaHPO_4 \cdot H_2O$, DCPA); 5) octacalcium phosphate ($Ca_8(HPO_4)_2(PO_4)_4 \cdot 5H_2O$, OCP); and 6) dicalcium phosphate dehydrate ($CaHPO_4 \cdot 2H_2O$, DCPD) (Musvoto et al., 2000; Montastruc et al., 2003; Uskoković, 2019). HA and TCP are thermodynamically stable but kinetically unfavorable (Nagano et al., 1996; Musvoto et al., 2000; Uskoković, 2019). The precipitation of polymorphs of calcium phosphates follows the Ostwald's rule of stages, in which the thermodynamically metastable crystal phases (e.g., ACP and DCPD) form in the initial stage and subsequently transform into thermodynamically more stable phases such as HA or TCP (Salimi et al., 1985; Nagano et al., 1996; Musvoto et al., 2000). ACP, OCP, DCPA, and DCPD can serve as intermediates during the crystallization of HA. In the supersaturated calcium phosphate solution with high magnesium concentration, formation of OCP and DCPA will be inhibited, whereas ACP and DCPD are more preferably to precipitate as the initial crystalline forms of calcium phosphates, with DCPD precipitating at pH values less than 7, and ACP precipitating at higher pH values (Salimi et al., 1985; Abbona et al., 1986; van Kemenade and de Bruyn, 1987; Abbona et al., 1988). Transition of ACP and DCPD into HA or TCP is relatively slow and is demonstrated to be significantly hindered by a high level of magnesium (Salimi et al., 1985; Abbona et al., 1988; Root, 1990; Musvoto et al., 2000). In seawater-urine system, HA, TCP, OCP and DCPA were therefore omitted from consideration, leaving only ACP and DAPD.

Calcium and magnesium carbonates. Calcite, aragonite, and vaterite are three forms of calcium carbonates that may crystallize, and calcite is reported to be the most thermodynamically stable form (Ni and Ratner, 2008). Two kinds of magnesium carbonates namely magnesite ($MgCO_3$) and nesquehonite ($MgCO_3 \cdot 3H_2O$), can occur, while only $MgCO_3$ can keep stable when the solution pH is less than 10.7 (Musvoto et al., 2000). The mixed carbonates of calcium and magnesium, dolomite ($CaMg(CO_3)_2$) and huntite ($CaMg(CO_3)_4$), are kinetically unfavorable (Musvoto et al., 2000).

Furthermore, Mg can co-precipitate with calcite as magnesium calcite, whereas the kinetics is not well understood (Berner, 1975).

In summary, precipitates included in the thermodynamic simulations are struvite, ACP ($Ca_9(PO_4)_6{\cdot}nH_2O$), DCPD ($CaHPO_4{\cdot}2H_2O$), calcite ($CaCO_3$), and magnesite ($MgCO_3$).

Laboratory-scale SUPR reactor

The SUPR reactor was made up from two concentric cylinders with a total operational volume of 840 mL, and the inner cylinder separated the reactor into a reaction zone and a separation zone (see Fig. S1). Additionally, the bottom of the reactor was equipped a collection funnel for harvesting precipitants. The reactor was fed with fresh seawater and urine (Table S1) from refrigerator continuously. Influent was introduced at the top port of the inner cylinder, while effluent was discharged through the outlet located at the upper part of the exterior cylinder. The harvested precipitates were separated from the liquid by filter membrane. Table S2 showed the effect of different pore sizes of the filter membrane on P recovery efficiency and filtration time, and 0.45-μm filter membrane was chosen to retain fine particles and biomass for laboratory analysis. Practically, considering that the filtrate can be recycled back to the reactor, 45-μm filter membrane is also acceptable.

Table S1 Properties of the fresh urine, ureolysed urine and seawater.

Parameters	Fresh Urine			Ureolysed Urine			Seawater		
	Mean	±SD	N	Mean	±SD	N	Mean	±SD	N
pH	6.32	0.38	20	9.24	0.13	20	8.08	0.090	6
Total Nitrogen (mg/L)	7300	1800	20	7100	1300	20	0.26	0.14	6
Ammonia (mg N/L)	330	75	20	6400	970	20	0.17	0.20	6
Total Phosphorus (mg/L)	310	120	20	240	100	20	—*		
Organic Carbon (mg/L)	5700	1800	6	2900	680	6	3.3	0.70	6
Inorganic Carbon (mg/L)	110	52	6	2900	470	6	24	0.87	6
Magnesium (mg/L)	42	9.0	6	1.2	0.70	6	1200	63	6
Calcium (mg/L)	120	36	6	13	9	6	470	86	6
Salinity (‰)	8.3	2.7	20	25	0.67	20	32	1.5	6
Conductivity (mS/cm)	14	4.5	20	39	2.2	20	48	0.81	6

Notes: * Below detection limit.

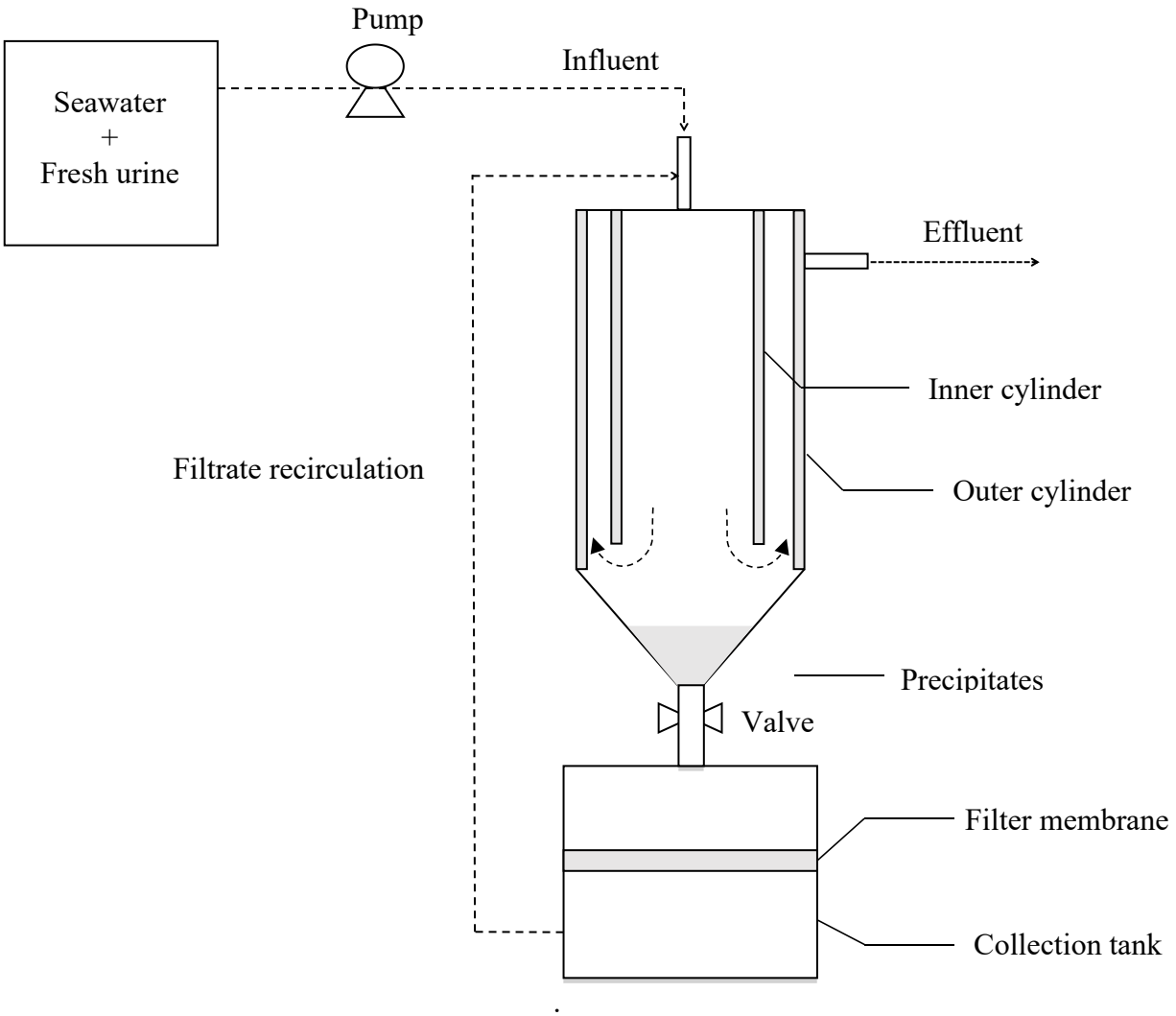

Fig. S1 Schematic diagram of SUPR reactor.

Table S2 The effect of different pore sizes of the filter membrane on P recovery.

Test	Pore size	Time for 90% filtration (min)	P recovery efficiency
1	100	1.5	18.2%
2	45	10	86.4%
3	38	28	93.8%
4	0.45	>60 (pressurized)	99.2%

Model components and parameters for urine nitrification model

Table S3 Definition of dissolved and particulate components in the model.

Number	Component	Definition	Unit
1	S_O	Dissolved oxygen	g O_2/m^3
2	S_S	Readily degradable organic substrate	g COD/m^3
3	S_{NH4}	Ammonium nitrogen	g N/m^3
4	S_{NO2}	Nitrite nitrogen	g N/m^3
5	S_{NO3}	Nitrate nitrogen	g N/m^3
6	I_{FA}	Free ammonia (FA)*	g N/m^3
7	I_{FNA}	Free nitrous acid (FNA) *	g N/m^3
8	X_{AOB}	Ammonium-oxidizing bacteria	g COD/m^3
9	X_{NOB}	Nitrite-oxidizing bacteria	g COD/m^3
10	X_H	Heterotrophic bacteria	g COD/m^3
11	X_S	Slowly degradable organic substrate	g COD/m^3
12	X_I	Inert, non-biodegradable organics	g COD/m^3

Notes: *The concentrations of FA and FNA were calculated based on the pH value and ammonium nitrogen or nitrite nitrogen concentration (Park et al., 2010).

Table S4 Process kinetic rate equations for the model.

Process	Kinetics rates expressions
1. Hydrolysis	$k_H \frac{X_S/X_H}{K_X + X_S/X_H} X_H$
2. Growth of AOB	$\mu_{AOB} \frac{S_{O2}}{K_{O2}^{AOB} + S_{O2}} \frac{S_{NH4}}{K_{NH4}^{AOB}\left(1 + \frac{I_{FNA}}{K_{I,FNA}^{AOB}}\right) + S_{NH4}\left(1 + \frac{I_{FNA}}{K_{I,FNA}^{AOB}} + \frac{I_{FA}}{K_{I,FA}^{AOB}}\right)} X_{AOB}$
3. Endogenous decay of AOB	$b_{AOB} \frac{S_{O2}}{K_{O2}^{AOB} + S_{O2}} X_{AOB}$
4. Growth of NOB	$\mu_{NOB} \frac{S_{O2}}{K_{O2}^{NOB} + S_{O2}} \frac{S_{NO2}}{K_{NO2}^{NOB}\left(1 + \frac{I_{FNA}}{K_{I,FNA}^{NOB}}\right) + S_{NO2}\left(1 + \frac{I_{FNA}}{K_{I,FNA}^{NOB}} + \frac{I_{FA}}{K_{I,FA}^{NOB}}\right)} X_{NOB}$
5. Endogenous decay of NOB	$b_{NOB} \frac{S_{O2}}{K_{O2}^{NOB} + S_{O2}} X_{NOB}$
6. Aerobic growth of X_H	$\mu_H \frac{S_{O2}}{K_{O2}^{H} + S_{O2}} \frac{S_S}{K_S + S_S} X_H$
7. Endogenous decay of X_H	$b_H \frac{S_{O2}}{K_{O2}^{H} + S_{O2}} X_H$

Table S5 Stoichiometric matrix for the model.

Variable	S_{O2}	S_S	S_{NH4}	S_{NO2}	S_{NO3}	S_{PO4}	X_S	X_{AOB}	X_{NOB}	X_H	X_I
Process	O_2	COD	N	N	N	P	COD	COD	COD	COD	COD
1		*1*					*−1*				
2	$-(3.43-Y_{AOB})Y_{AOB}$		$-i_{NBM}-1/Y_{AOB}$	$1/Y_{AOB}$		$-i_{PBM}$		*1*			
3	$-(1-f_I)$		$i_{NBM}-i_{NXI}/f_I$			i_{PBM}		*−1*			f_I
4	$-(1.14-Y_{NOB})Y_{NOB}$		$-i_{NBM}$	$-1/Y_{NOB}$	$1/Y_{NOB}$	$-i_{PBM}$			*1*		
5	$-(1-f_I)$		$i_{NBM}-i_{NXI}/f_I$			i_{PBM}			*−1*		f_I
6	$-(1-Y_{H,O2})Y_{H,O2}$	$-1/Y_{H,O2}$	$-i_{NBM}$			$-i_{PBM}$				*1*	
7	$-(1-f_I)$		$i_{NBM}-i_{NXI}/f_I$			i_{PBM}				*−1*	f_I

Table S6 Kinetic and stoichiometric parameters of the model.

	Parameter	Definition	Values	Unit	Source
Ammonium oxidizing bacteria (AOB)	Y_{AOB}	yield coefficient for AOB	0.15	g COD/g N	Wiesmann (1994)
	μ_{AOB}	maximum growth rate of AOB	0.054	h^{-1}	Mackey et al. (2016)
	b_{AOB}	endogenous decay rate of AOB	0.0054	h^{-1}	Wiesmann (1994)
	K_{O2}^{AOB}	S_{O2} affinity constant for AOB	0.6	g DO/m^3	Wiesmann (1994)
	K_{NH4}^{AOB}	S_{NH4} affinity constant for AOB	2.4	g N/m^3	Wiesmann (1994)
	$K_{I,FA}^{AOB}$	FA inhibition concentration for AOB	10	g FA/m^3	Park et al. (2010)
	$K_{I,FNA}^{AOB}$	FNA inhibition concentration for AOB	0.5	g FNA/m^3	Park et al. (2010)
Nitrite oxidizing bacteria (NOB)	Y_{NOB}	yield coefficient for NOB	0.041	g COD/g N	Wiesmann (1994)
	μ_{NOB}	maximum growth rate of NOB	0.045	h^{-1}	Mackey et al. (2016)
	b_{NOB}	endogenous decay rate of NOB	0.0025	h^{-1}	Wiesmann (1994)
	K_{O2}^{NOB}	S_{O2} affinity constant for NOB	2.2	g DO/m^3	Wiesmann (1994)
	K_{NO2}^{NOB}	S_{NO2} affinity constant for NOB	5.5	g N/m^3	Wiesmann (1994)
	$K_{I,FA}^{NOB}$	FA inhibition concentration for NOB	0.75	g FA/m^3	Park et al. (2010)
	$K_{I,FNA}^{NOB}$	FNA inhibition concentration for NOB	0.1	g FNA/m^3	Park et al. (2010)
Heterotrophic bacteria (H)	$Y_{H,O2}$	aerobic yield coefficient for X_H	0.54	g COD/g COD	Gujer et al. (1999)
	μ_H	maximum growth rate of X_H	0.3	h^{-1}	Wiesmann (1994)
	b_H	endogenous decay rate of X_H	0.008	h^{-1}	Wiesmann (1994)
	k_H	hydrolysis rate constant	0.125	h^{-1}	Gujer et al. (1999)
	K_X	hydrolysis saturation constant	1	g COD/g COD	Gujer et al. (1999)
	K_{O2}^{H}	S_{O2} affinity constant for X_H	0.2	g DO/m^3	Gujer et al. (1999)
	K_S	S_S affinity constant for X_H	2.0	g COD/m^3	Gujer et al. (1999)
Other parameters	i_{NBM}	Nitrogen content of biomass	0.07	g N/g COD	Henze et al. (2000)
	i_{NXI}	Nitrogen content of X_I	0.02	g N/g COD	Henze et al. (2000)
	i_{PBM}	Phorsphorus content of biomass	0.02	g P/g COD	Henze et al. (2000)
	f_I	Fraction of X_I in biomass decay	0.10	g COD/g COD	Henze et al. (2000)

Batch kinetic tests and modeling

During phases IV, V and VI, a set of batch tests were conducted to study the kinetics of ureolysis and P precipitation. Attached sludge obtained from the SUPR reactor was inoculated into 1 L FU-seawater mixtures with different S/U ratios (i.e. 5:1, 7:1, and 9:1). TAN, TSP, and magnesium concentrations of the mixtures were closely monitored. A previous developed kinetic model was applied to simulate the kinetics (Tang et al., 2015). The kinetics of microbial ureolysis were determined by a biomass-dependent Michaelis-Menten equation (Eq. (S1)):

$$v = \frac{V_m \cdot [Urea]}{K_m + [Urea]}[B] \quad , \qquad (S1)$$

where v is the ureolysis rate (mmol/L/h); V_m is the maximum specific rate of ureolysis (mmol/cell/h); [Urea] is the concentration of urea (mmol/L); K_m is the half-saturation substrate concentration (mmol/L) at which $v = 0.5 \cdot V_m \cdot [B]$; and [B] is the bacterial abundance (cell/L).

A previously developed kinetic model (Musvoto et al., 2000) was modified and applied in this study to simulate the phosphate precipitation kinetics, as well as the weak acid/base equilibria. Forward and reverse reactions were considered in the model simulation, from which the crystallization process was predicted by applying the concentration changes as a function of time. The precipitation rate of struvite (MAP) was determined in the model simulation from Eq. (S2):

$$\frac{d[MgNH_4PO_4]}{dt} = K_{MAP}((Mg^{2+})^{\frac{1}{3}}(NH_4^+)^{\frac{1}{3}}(PO_4^{3-})^{\frac{1}{3}} - K_{sp}^{\frac{1}{3}})^3 \quad , \qquad (S2)$$

where (Mg^{2+}), (NH_4^+), and (PO_4^{3-}) are the activity of each ion in solution, K_{sp} is the apparent solution product of MAP; and K_{MAP} is the apparent precipitation rate constant. Other potential precipitates considered in this model are ACP ($Ca_9(PO_4)_6 \cdot nH_2O$), calcite ($CaCO_3$), and magnesite ($MgCO_3$). The kinetic parameters were taken from (Dai et al., 2014).The model was run on computer simulation program Aquasim 2.1.

As shown in Fig. S2 and Table S7, a strong concordance was observed between the experimental and simulation results ($R^2 > 0.95$, except for Mg under S/U ratio of 9:1).

Table S7 The coefficient of determination (R^2) and significance (p value) of kinetic modeling results.

Datasets	5:1		7:1		9:1	
	R^2	p	R^2	p	R^2	p
TAN	0.998	5.6E-14	0.998	2.7E-13	0.995	7.9E-12
P	0.99	1.2E-11	0.99	3.1E-10	0.99	1.6E-10
Mg	0.96	1.6E-07	0.96	1.4E-07	0.81	0.00014

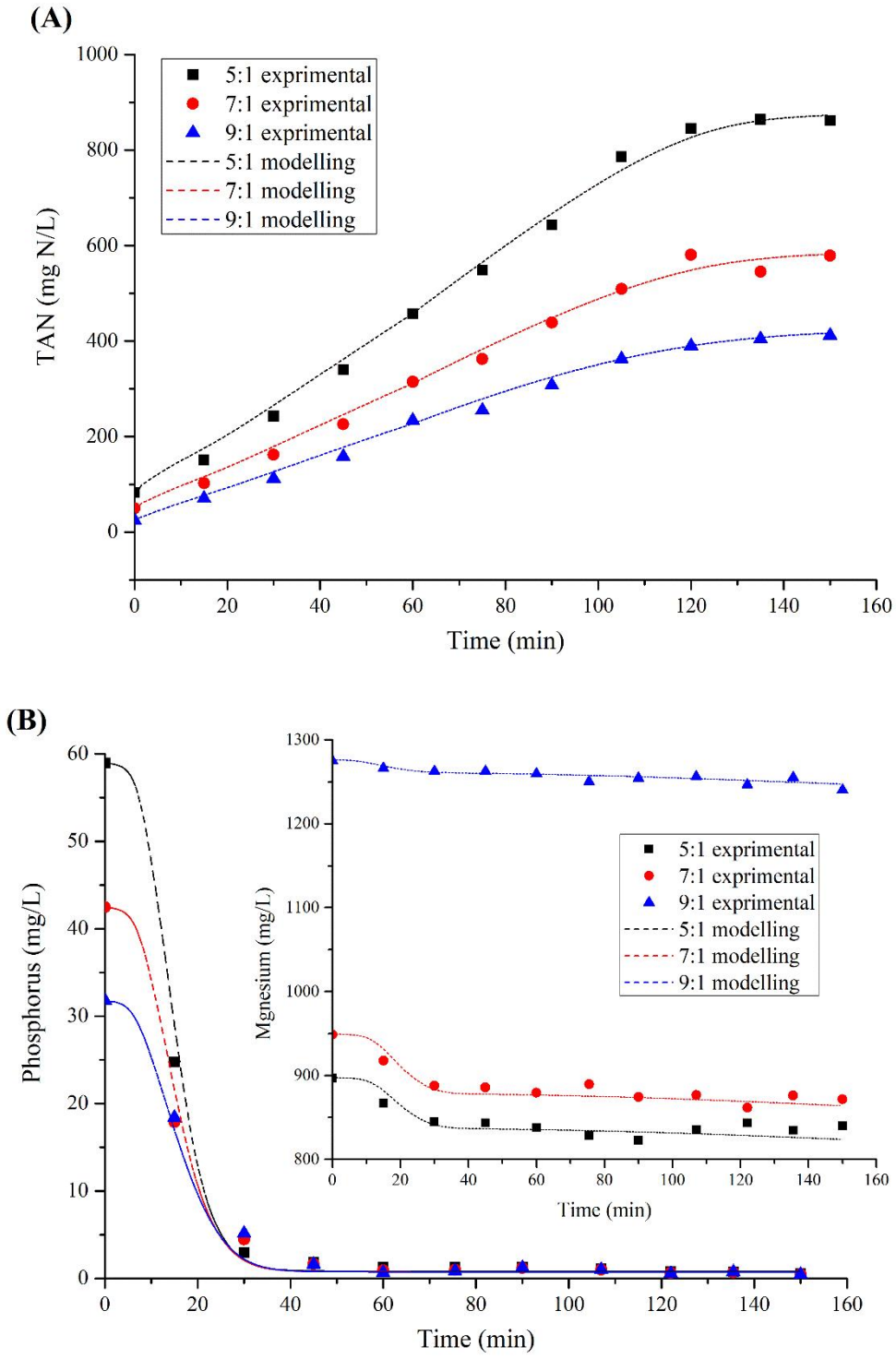

Fig. S2 Kinetics of (A) ureolysis and (B) P precipitation in phases IV, V and VI with S/U ratios of 5:1, 7:1 and 9:1.

References

Abbona F, Lundager Madsen H E, Boistelle R (1986). The initial phases of calcium and magnesium phosphates precipitated from solutions of high to medium concentrations. Journal of Crystal Growth, 74(3): 581–590

Abbona F, Lundager Madsen H E, Boistelle R (1988). The final phases of calcium and magnesium phosphates precipitated from solutions of high to medium concentration. Journal of Crystal Growth, 89(4): 592–602

Berner R A (1975). The role of magnesium in the crystal growth of calcite and aragonite from sea water. Geochimica et Cosmochimica Acta, 39(4): 489–504

Dai J, Tang W T, Zheng Y S, Mackey H R, Chui H K, Van Loosdrecht M C M, Chen G H (2014). An exploratory study on seawater-catalysed urine phosphorus recovery (SUPR). Water Research, 66: 75–84 doi:10.1016/j.watres.2014.08.008

Gujer W, Henze M, Mino T, Van Loosdrecht M (1999). Activated sludge model No. 3. Water Science and Technology, 39(1): 183–193

Henze M, Gujer W, Mino T, van Loosdrecht M C (2000). Activated sludge models ASM1, ASM2, ASM2d and ASM3. London: IWA publishing

Mackey H R, Rey Morito G, Hao T, Chen G H (2016). Pursuit of urine nitrifying granular sludge for decentralised nitrite production and sewer gas control. Chemical Engineering Journal, 289: 17–27

Mamais D, Pitt P A, Cheng Y W, Loiacono J, Jenkins D (1994). Determination of ferric chloride dose to control struvite precipitation in anaerobic sludge digesters. Water Environment Research, 66(7): 912–918

Montastruc L, Azzaro-Pantel C, Biscans B, Cabassud M, Domenech S (2003). A thermochemical approach for calcium phosphate precipitation modeling in a pellet reactor. Chemical Engineering Journal, 94(1): 41–50

Musvoto E V, Wentzel M C, Ekama G A (2000). Integrated chemical-physical processes modelling - II. Simulating aeration treatment of anaerobic digester supernatants. Water Research, 34(6): 1868–1880

Nagano M, Nakamura T, Kokubo T, Tanahashi M, Ogawa M (1996). Differences of bone bonding ability and degradation behaviour in vivo between amorphous calcium phosphate and highly crystalline hydroxyapatite coating. Biomaterials, 17(18): 1771–1777

Ni M, Ratner B D (2008). Differentiation of calcium carbonate polymorphs by surface analysis techniques - an XPS and TOF-SIMS study. Surface and Interface Analysis, 40(10): 1356–1361

Park S, Bae W, Rittmann B E (2010). Operational boundaries for nitrite accumulation in nitrification based on minimum/maximum substrate concentrations that include effects of oxygen limitation, pH, and free ammonia and free nitrous acid inhibition. Environmental Science & Technology, 44(1): 335–342

Root M J (1990). Inhibition of the amorphous calcium phosphate phase transformation reaction by polyphosphates and metal ions. Calcified Tissue International, 47(2): 112–116

Salimi M, Heughebaert J, Nancollas G (1985). Crystal growth of calcium phosphates in the presence of magnesium ions. Langmuir, 1(1): 119–122

Tang W T, Dai J, Liu R, Chen G H (2015). Microbial ureolysis in the seawater-catalysed urine phosphorus recovery system: Kinetic study and reactor verification. Water Research, 87: 10–19

Tilley E, Atwater J, Mavinic D (2008). Effects of storage on phosphorus recovery from urine. Environmental Technology, 29(7): 807–816

Uskoković V (2019). Disordering the disorder as the route to a higher order: incoherent crystallization of calcium phosphate through amorphous precursors. Crystal Growth & Design, 19(8): 4340–4357

van Kemenade M J J M, de Bruyn P L (1987). A kinetic study of precipitation from supersaturated calcium phosphate solutions. Journal of Colloid and Interface Science, 118(2): 564–585

Wiesmann U (1994). Biological nitrogen removal from wastewater. Advances in Biochemical Engineering/Biotechnology, 51: 113–154